WOOD RESEARCH
54 (3): 2009
33-44

TOMOGRAPHIC INVESTIGATIONS OF WOOD FROM MACROSCOPIC TO MICROSCOPIC SCALE

David Mannes, Peter Niemz
Institute for Building Materials, Wood Physics, ETH Zurich, Switzerland

Eberhard Lehmann
ASQ, Neutron Imaging and Activation Group (NIAG),
Paul Scherrer Institut, Villigen PSI, Switzerland Villigen PSI, Switzerland

/Based on an article presented at the 15 th International Symposium on Nondestruktive Testing of Wood, September 9-12, 2007 Dulut, MN (USA)/

ABSTRACT

Computed tomography based on transmission measurements of penetrating ionising radiation can be a powerful tool for the characterisation of wood and wood based materials. This includes not only structural appraisal but also dynamic processes and interaction with different substances (e.g. water, repellents, preservatives, adhesives, etc.). The different kinds of radiation on which these tomography methods are based show large variations concerning their respective sensitivity for the elements concerned and thus different fields of application: (1) X-ray tomography can be used on a macroscopic level, where wooden objects of several tens of centimetres can be examined, while (2) synchrotron radiation can be used for microscopic investigations down to the cell wall level. (3) Imaging with thermal and cold neutrons with their high sensitivity towards light elements such as hydrogen on the other hand is thus particularly suitable for investigations on the interactions between wood and hydrogenous substances (water, adhesive, …). In the presented work, tomographic methods based on the three named radiation types will be characterised with regards to their application area on practical examples ascertained at the facilities of the Paul Scherrer Institut Villigen (Switzerland).

KEY WORDS: non-destructive testing, X-ray tomography, neutron tomography, synchrotron microtomography

INTRODUCTION

Computed tomography (CT) is a method producing virtual cross-sectional images of the inner structure of an object. These are based in most cases on transmission images of the aforesaid object made from different projections. The method itself is based on the theoretical works by Radon in 1917 (Brooks and Di Chiro 1975). As practical method, CT was developed in the 1960s by Cormack (1963) and Hounsfield (1980) for medical diagnostics using X-ray for the acquisition of the raw images and has become a widespread standard method in numerous fields like material

research, archaeology, engineering, etc. A short overview on the utilisation of CT in the field of wood research is given by Bucur (2003).

Wood as a natural and organic material has a complex structure which is very distinctive over several hierarchical levels, from the inner composition of the cell wall on a submicro or even nanolevel, over the structure of the cells in the plant tissue on a microscopic level to the alignment of different tissues (parenchyma, late / spring wood) on a macroscopic level.

For many problems dealing either with the inner structure or processes within the timber an appropriate investigation can only be conducted in the undisturbed / uninfluenced material. Computed tomography based on ionising radiation can be an appropriate method for non-destructive investigation of wood.

In this work tomography on different scale levels will be presented using the facilities (standard X-ray, neutron and synchrotron radiation) available at the Paul-Scherrer-Institut (PSI) in Villigen, CH.

MATERIAL AND METHODS

Material

X-ray

For the X-ray tomography a wedge shaped section of Norway spruce (*Picea abies*) with wood defects visible on the surface was used. The sample was sawn of a log segment in order to obtain a section featuring wood from the core to the bark as well as knots and wood defects. The specimen was sized ca. 20 cm for the radial surfaces, a height of 20 cm and a wedge angle of ca. 60°.

Cold neutrons

For the tomography with cold neutrons two rectangular specimens were used. One was oak wood (*Quercus spec.*) with dimensions of 10 x 10 x 30 mm the other was a specimen composed of two beech wood parts joined with a 1K-PUR adhesive with similar dimensions than the oak sample.

Synchrotron

For the micro-tomography at the synchrotron radiation source a turning lathe was used to prepare cylindrical specimens with a radius of 1 and 3 mm and a height of 10 to 15 mm from bigger beech wood (*Fagus sylvatica*) cubes.

The samples used for the three experiments were conditioned before the tests in room climate to prevent dimensional changes during the measurements due to moisture variances.

Experimental setup

The common point of all experiments was the basic setup principle. Radiation is led from a well defined source on a specimen, which is positioned on a turning table. Behind the sample a detector is registrating the transmitted part of the beam distribution. The detector-system used was very similar in all three cases. The system consists of a scintillator, which converts the incoming radiation into visible light, which is then reflected by a mirror via a lens system on a CCD-camera (Fig. 1). The scintillators differ only in the material, which is used as an absorbing agent for the respective radiation. The basic setup of such a scintillator CCD-camera system was described by Pleinert et al (1997).

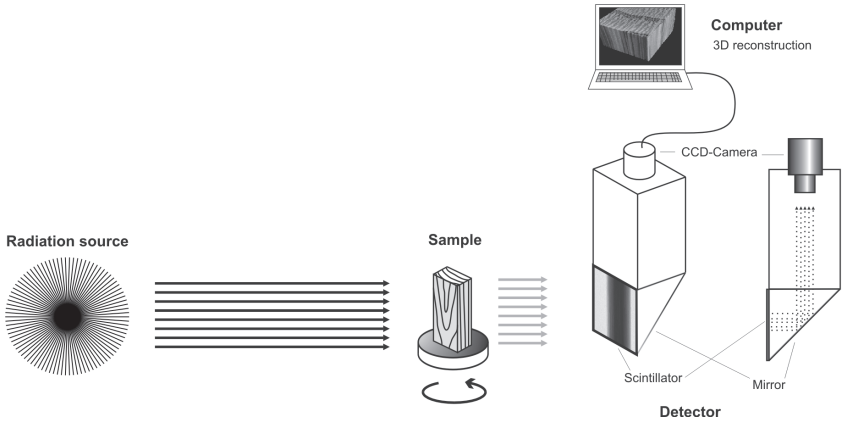

Fig. 1: Basic experimental setup; radiation is led from the source in a parallel beam on the sample positioned on a turning table; the transmitted beam is registered by a detector consisting of a scintillator, a mirror and a CCD-Camera; the raw data are transmitted to a computer performing the 3D reconstruction

The other common point of the methods presented in this work is the general working principle of computed tomography (CT). The presented examples were produced on basis of attenuation-based transmission images from an object made from different viewing angles using a parallel beam. As a rule, these projections were made over an area of 180. The images are subsequently used for the reconstruction of tomograms, which is usually done with standard software tools, like *Octopus* (*XRayLab*, B *(http://www.xraylab.com/)*), which was used for the reconstruction of the data from the X-ray and neutron tomography. The reconstruction of the synchrotron data was done with software developed at PSI especially for the used tomography-beamline at the "Swiss Light Source".

The main difference between the three employed methods is the radiation used to generate the transmission images and the materials used for the detectors. Synchrotron radiation forms, e.g. when electrons are forced by magnetic fields to deviate from their flight direction, as it is the case in ring accelerators. This force, which acts on the electron induces an emission of electromagnetic radiation, the synchrotron light. X-rays are produced by the deceleration of electrons. Here electrons are first accelerated from a cathode on an anode where they are strongly decelerated, which causes anew the emission of electromagnetic radiation in from of X-rays. Neutron radiation, which was used for the present investigation was produced within the spallation neutron source SINQ (Bauer 1998). Protons are accelerated and led onto a heavy metal target. The collision of the protons with nuclei within the target causes the spallation of neutrons. The resulting high energy neutrons have to be slowed down through moderation in a tank filled with heavy water to thermal and cold neutrons.

The X-ray tomography was conducted at the NEUTRA-beamline dedicated to experiments with thermal neutrons, which is also equipped with an X-ray tube, which can be positioned at the start of the outer collimator using with exception of the source position the same experimental setup as described in Lehmann et al. (1999). For the presented tomography a voltage of 80 kV, current of 45mA and an exposure time of 5s were used. 401 images were made over 180°. The scintillator used in the detector system was 300 µm gadox-scintillator.

For the tomography with cold neutrons at the ICON-beamline the micro-tomography-setup described in Lehmann et al. (2007) was used, which yields a nominal pixel size of 13.5µm resulting in an actual resolution of 30 to 50 µm depending on the used scintillator thickness and material.

The exposure time was 50s and 451 projections were made over 180°. As scintillator a 50 µm LiF-scintillator was used.

The tomography with synchroton radiation was performed at the TOMCAT-beamline of the Swiss Light Source (SLS) (Stampanoni et al. 2007). The beam energy was controlled with a double-crystal-monochromator to an energy of 8keV. For the tomography a total of 1501 projections were made over 180°. The Field of view was 1.43 x 1.43 mm resulting in a nominal pixel size of 0.7 µm using a YAG:Ce 20 µm scintillator.

An overview on the experimental setups can be found in Tab. 1.

Tab. 1: Overview of the experimental setup used at the different beamlines

Facility	Beam property / energy	Exposure time	Number of projections	Field of View	CCD-Camera	Nominal pixel size
X-TRA at NEUTRA	X-ray with up to 80 kV (full spectrum)	5 s	401	27cm	1024 x 1024 pixel (16bit)	275 µm
ICON	Cold neutrons with energy between 4meV and 0.5meV (full spectrum)	50 s	451	27mm	2048 x 2048 pixel (16bit)	13.5 µm
TOMCAT	Synchrotron radiation with 8keV (mono-ergetic)	700 ms	1501	1.5mm / 3.5mm	2048 x 2048 pixel (14bit)	0.75 µm / 1.5 µm

General principle of transmission imaging

Transmission images represent shadow images of an object within the beam. Depending on the constitution and composition of the object the beam is attenuated to a certain degree. The relationship between the incident beam and the transmitted one and thus to a certain degree weakened beam intensity complies in first order with the exponential attenuation law and can be described as follows:

$$I = I_0 \cdot e^{-\Sigma \cdot d} \tag{1}$$

Where:
I_0 = incident intensity of the neutron beam [grey levels]
I = transmitted intensity of the neutron beam [grey levels]
Σ = attenuation coefficient [cm^{-1}]
d = sample thickness [cm]

This relationship is the same independent of the radiation type and differs only in the denomination of the attenuation coefficient or macroscopic cross-section, which is usually labelled Σ for neutrons and µ for interactions with X-ray photons.

Based on equation (1), the attenuation coefficient Σ can be calculated by:

$$\Sigma = \frac{\ln(\frac{I_0}{I})}{d} \qquad [cm^{-1}] \tag{2}$$

The attenuation coefficient or macroscopic cross-section is the parameter which describes the probability of interaction between the beam and the irradiated material. This comprises scattering of the particles by the atoms within the material as well as the absorption of the

particles. Thus exponential attenuation law (cf. equation 1) complies only in first order especially if materials with high scattering ability are involved. This necessitates the implementation of correction methods if a quantitative evaluation is needed (cf. Hassanein et al. 2006). The attenuation coefficient is also the parameter in which the presented methods vary. This is on one hand caused by the different interaction of the beam with the atoms within the specimen. While X-ray photons interact with the electrons within the electron shells of the atoms the neutrons interact with the nuclei of the present atoms. As a consequence the attenuation coefficient of X-ray for different elements is strongly correlated to the atomic number of the elements within the periodic system and thus increasing with higher atomic numbers. The attenuation coefficient of neutrons shows no clear correlation but is very high for some light elements like hydrogen and very low for heavier elements like lead. Furthermore the attenuation coefficient is also depending on the energy of the radiation. It hence shows as a general rule higher values for lower energies of the same radiation type, being e.g. conspicuously higher for cold neutrons than for the higher energetic thermal neutrons.

Working area / range

The attenuation coefficient for beech wood for the different radiation types diverges varies considerable with values of μ_S = 4.6 cm^{-1} for synchrotron radiation, Σ_C = 1.5 cm^{-1} for cold neutrons, Σ_T = 1 cm^{-1} for thermal neutrons and μ_X = 0.1 cm^{-1} for X-ray (with 160 kV). This divergence between the attenuation coefficients necessitates the definition of a working range for each method. The working range meaning the dimensional limits of a specimen, which have to be adhered to ascertain that the experiment can be conducted properly, depends on the attenuation coefficient and the sensitivity of the utilised detector-system. To be distinguishable as a proper signal it must differ at least one noise level from the upper and lower limit of the dynamic range of the detector (e.g. 16bit = 65536 grey levels). For the presented detector-systems a noise level of ΔI = 2% was assumed and the upper and lower limits of the detectable attenuation were calculated under consideration of equation (1):

lowest detectable attenuation

$$(\sum * d)_{\min} = \ln(\frac{I_0}{I}) = \ln(\frac{100}{98}) = \ln(1.02) = 0.02 \quad (3)$$

highest detectable attenuation:

$$(\sum * d)_{\max} = \ln(\frac{I_0}{I}) = \ln(\frac{100}{2}) = \ln(50) = 3.91 \quad (4)$$

With the attenuation coefficients derived from transmission images the minimal and maximal thickness for a specimen which can be examined with the different methods can now be calculated:

Minimal detectable specimen thickness:

$$d_{\min} = \frac{0.02}{\sum}$$

Maximal detectable specimen thickness:

$$d_{\max} = \frac{3.91}{\sum}$$

The resulting working areas cover 4 orders of magnitude from approximately 40 µm (for synchrotron radiation (8 keV) to 40 cm (X-ray with 160 kV) (Fig. 2).

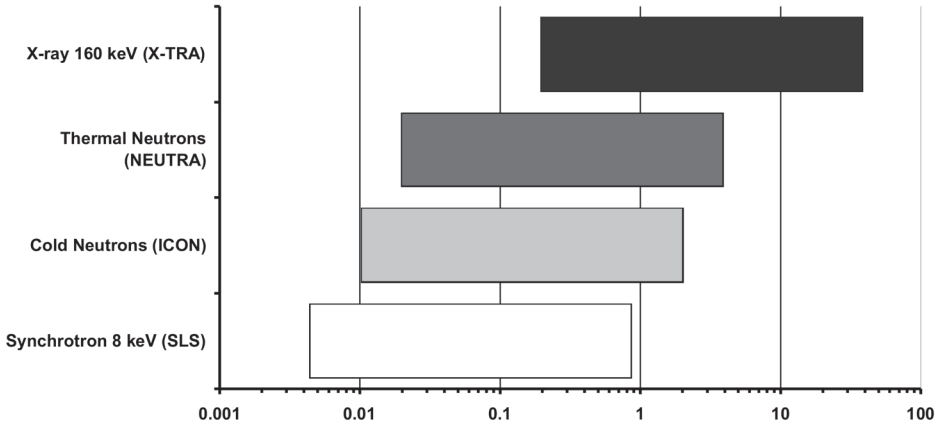

Fig. 2: Working range for X-ray (160 kV) (black), thermal neutrons (grey), cold neutrons (light grey) and synchrotron radiation (8keV) (white) for beech wood on a logarithmic scale

RESULTS

X-ray

In the 3D reconstruction of the wedge shaped spruce wood section certain bigger features can be distinguished, like an occlusion in the inner third of the cross section. Alongside a resin pocket and a small knot can be observed at the same height as the occlusion. The tree ring structure can only be clearly distinguished in the inner part of the cross-section, where the size of the annual rings is higher and principally due to higher density variations between spring and late wood. In the outer part beyond the resin pocket the tree ring structure can scarcely be delimited.

The features, which are discernable in the X-ray tomography are on a macroscopic level and are comparable to what could be seen with the bare eye (Fig. 3) but the virtual slices can be observed at arbitrary positions. Within the reconstructed model of the wedge shaped spruce wood section an occlusion is visible in the inner third of the cross section (Fig. 4). At the same height within the specimen also a resin pocket and a small knot starting almost in the core are discernable. The three-dimensional reconstruction makes it possible to ascertain the constitution of the occlusion as well as the extension of the resin pocket in the axial direction (Fig. 5). This lack of resolution is on one hand due to the relative low sensitivity of X-ray for wood and on the other hand on the size of the field of view, which is necessary to fit a specimen of a certain size. The size of the field of view determines the pixel size, within the projections. The pixel size could be reduced by the utilization of a smaller field-of-view and the sensitivity of the X-ray might be enhanced by lower energies. This would on the other hand mean, that only smaller specimens could be examined, although the possibility to use relatively big specimens is one of the advantages of X-ray tomography. Furthermore it is easily available in comparison to the other two methods.

Possible applications comprise the investigation of real size objects and valuables (e.g. antique wood instruments, statues, etc.) as well as the classification of raw material for the production of wood based materials.

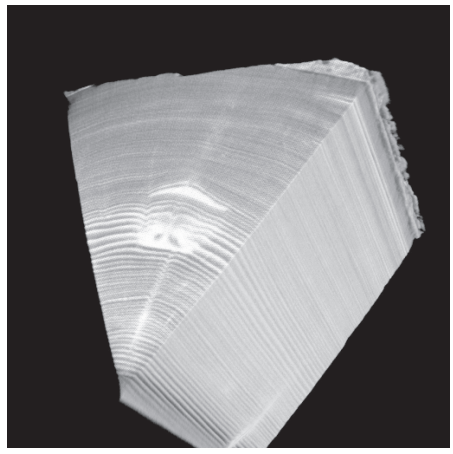

Fig.3: 3D rendered view (X-ray CT) of a wedge-shaped spruce specimen. The grey levels correspond to the varying attenuation within different parts of the object

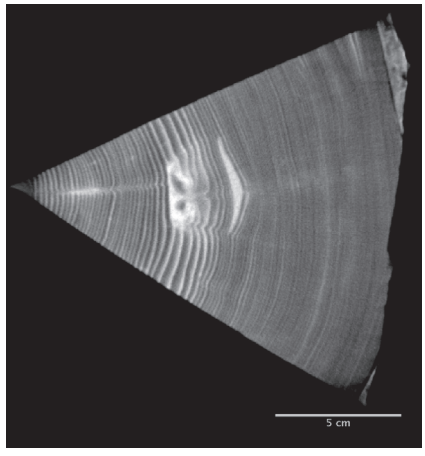

Fig. 4: Reconstructed X-ray tomogram through a spruce wood sample; at the limit of the inner third an occlusion is visible as well as a resin pocket further to the bark

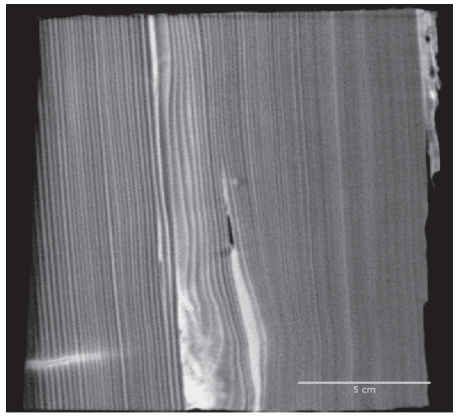

Fig. 5: Reconstructed radial X-ray slice through a spruce wood sample; the extension in axial direction of an occlusion as well as of a resin pocket can be seen; also small knot starting from the core and ending after few centimetres is visible

NEUTRON RADIOGRAPHY

Oak wood specimen

The tomography of the oak sample made with cold neutrons is on an intermediate scale-level, going beyond the macroscopic level and almost reaching a microscopic level. Features, which are discernable comprise the big spring wood vessels as well as medium sized and small vessels. Denser areas containing mainly fibres can be distinguished from less dense tracheidal zones around the vessels. The big wood rays are visible as well. The rendered 3D-model allows the determination of the vessel pathway and linkage in axial direction (Fig. 7). With the exception of the vessels individual cells or other microscopic features cannot be observed.

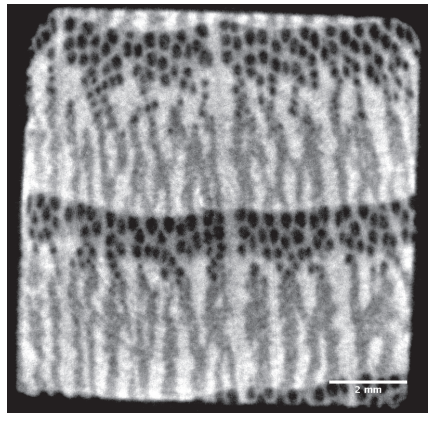

Fig. 6: Tomogram accomplished with cold neutrons made of an oak sample; water conducting areas can easily be distinguished from fibre tissue and wood rays

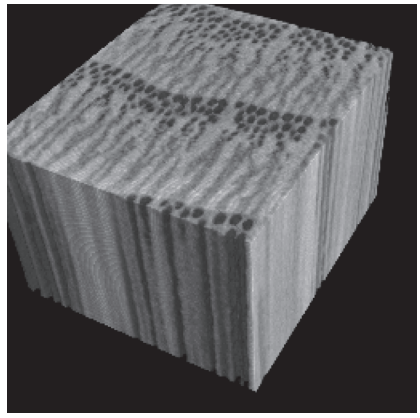

Fig. 7: Rendered 3D model of the neutron tomography showing the axial distribution of the different tissues

Adhesive joint

Although the limitations of the individual annual rings are clearly visible in tomogram of the beech sample glued with PUR-adhesive it is not possible to discern single vessels within the tissue so that it more or less remains on o macroscopic level. On the other hand wood rays as well as the adhesive joint can be observed Fig. 8. Besides these anatomic details the most conspicuous feature is the adhesive joint. The distribution and allocation of the PUR-adhesive can be discerned between the two wood halves. The good distinguishability is due to the high content of hydrogen within the adhesive for which neutrons are more sensitive than the other two methods. Thus the interaction with hydrogenous substances as adhesive, resins, coatings or water represents one of the main applications of the method. Currently a project deals with the penetration behaviour of various adhesives using the different methods.

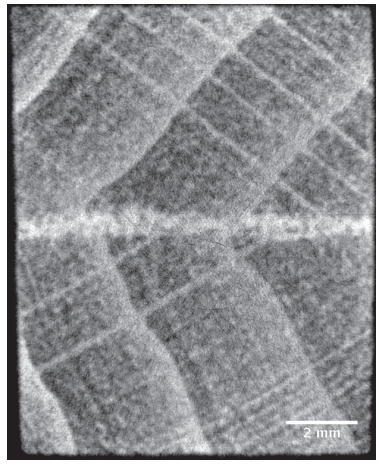

Fig.8: Neutron tomogram trough a beech wood sample with a 1K-PUR adhesive joint , the glue line is obvious as neutrons highly sensitive for hydrogen

Synchrotron radiation

In the micro-tomography of the beech sample even microscopical features are visible. Alongside the relatively large vessels and wood rays individual fibres can be discerned to their cell wall level (Fig. 9). The rendered 3D-modell shows also features within the cell wall namely pits between vessels and fibres respectively other vessels (Fig. 10) as well as the joints between vessel elements (Fig. 11). The cell wall itself appears homogenous and hence the individual cell wall layers are not discernable. A possible approach to make structures within the cell wall perceptible might either be the utilisation of the phase-contrast phenomenon or a smaller field-of-view implying also optics with higher magnification. These options are already available at the TOMCAT-beamline but were not employed in the presented measuring campaign.

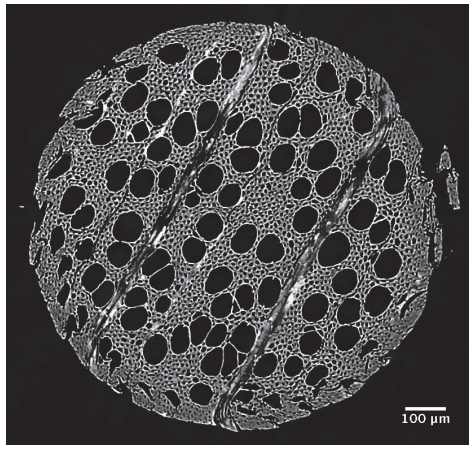

Fig. 9: Reconstructed cross-section through a beech specimen (diameter 1mm); vessels and wood rays can be seen embedded in the fibre tissue. In the outer area of the specimen damage caused by machining during sample preparation

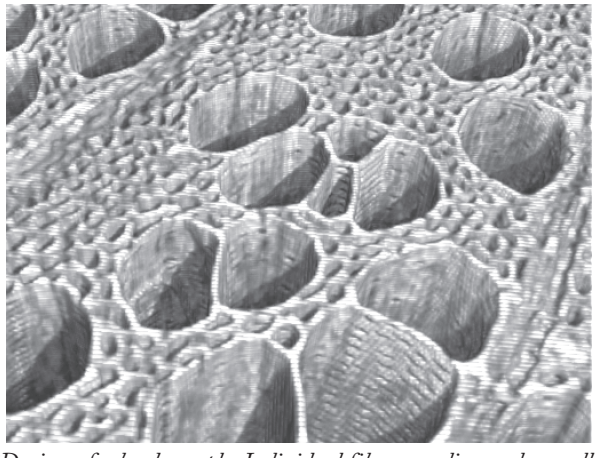

Fig. 10: Rendered 3D view of a beech sample. Individual fibres can discerned as well as connecting pits in the vessel walls

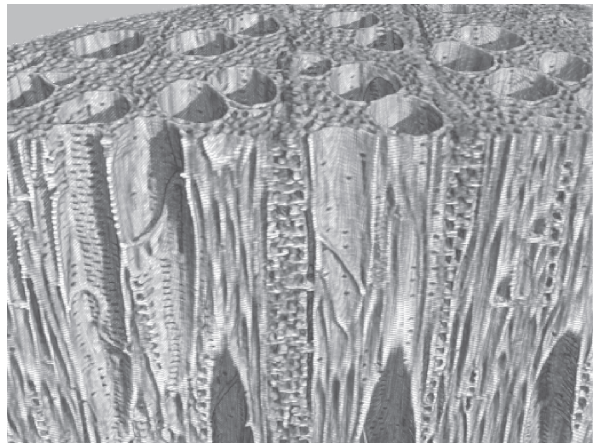

Fig. 11: Virtual tangential view inside the beech sample. Pits and the joints between the vessel elements can be seen

CONCLUSIONS

Every of the presented methods has its proper application fields and specific limitations. It is thus important to determine the right method to attain the goals of the respective research project even though the methods show a certain overlap for the working area (specimen size). X-ray tomography is applicable within a wide range of applications, making investigations of big samples up to several dm possible. The investigation of smaller objects is however limited by its sensitivity for wood. The sensitivity can indeed be improved by the utilisation of lower energies, which would on the other hand result in longer exposure times. This is on the other hand always depending on the limitations of the specific X-ray tube and experimental setup (e.g. collimator windows, etc.) .The main working area still will be on a macroscopic level. Tomography using cold neutrons is well suited to make investigations on an intermediate scale close to a microscopic level. It yields good results on structural features but its strong point would be in the localisation and possible quantification of hydrogenous substances like adhesives, varnish or water within the sample. This fact is due to its high sensitivity for hydrogen, which on the other hand limits the specimens to a size of few cm. The micro-tomography using synchrotron-radiation goes further and is really on a microscopic level, providing information on microscopic details like pits, certain cell wall features, etc. With this method highly resolved images can be obtained on a microscopical level almost comparable toe SEM-images concerning their quality but on a non-destructive way (if the sample preparation is not taken into consideration). Still this method is limited to sample sizes of less than 1 cm and a certain effort for the sample preparation has to be accepted.

ACKNOWLEDGEMENT

The authors want to thank the team from the TOMCAT-beamline for their support during the measurements namely Dr. M. Stampanoni, Dr. F. Marone and G. Mikuljan for the help with the sample preparation for the synchrotron experiments.

REFERENCES

1. Bauer, G.S., 1998: Operation and development of the new spallation neutron source SINQ at the Paul Scherrer Institut. Nuclear instruments and methods in physics research section B- beam interactions with materials and atoms 139(1-4): 65-71
2. Brooks, R.A., Di Chiro, G., 1975: Theory of image reconstruction in computed tomography. Radiology 117: 561-572
3. Bucur, V., 2003: Techniques for high resolution imaging of wood structure: A review. Measurement Science & Technology 14(12): R91-R98
4. Cormack, A.M., 1963: Representation of a function by its line integrals, with some radiological applications. Journal of Applied Physics. 34(9): 2722-2727
5. Hassanein, R., de Beer, F., Kardjilov, N., Lehmann, E., 2006: Scattering correction algorithm for neutron radiography and tomography tested at facilities with different beam characteristics. Physica B - condensed matter 385-86: 1194-1196 Part 2
6. Hounsfield, G., 1980: Computed medical imaging, Science 210(4465): 22-28
7. Lehmann, E.H., Vontobel, P., Wiezel, L., 2001: Properties of the Radiography Facility NEUTRA at SINQ and its Potential for Use as European Reference Facility. Nondestructive Testing and Evaluation 16:191202
8. Lehmann, E.H., Frei, G., Kühne, G., Boillat, P., 2007: The micro-setup for neutron imaging: a major step forward to improve the spatial resolution. Nuclear instruments and methods in physics research 576: 389-396
9. Pleinert, H., Lehmann, E., Körner, S., 1997: Design of a new CCD-camera neutron radiography detector. Nuclear instruments and methods in physics research 399: 382-390
10. Stampanoni, M., Groso, A., Isenegger, A., Mikuljan, G., Chen, Q., Meister, D., Lange, M., Betemps, R., Henein, S., Abela, R., 2007: TOMCAT: a beamline for tomographic microscopy and coherent radiology experiments. Synchrotron radiation instrumentation, PTS 1 and 2. 879: 848-851

David Mannes, PhD
ETH Zurich
Institute for Building Materials, Wood Physics
Schafmattstrasse 6
8093 Zurich
Switzerland

Eberhard Lehmann
ASQ, Neutron Imaging and Activation Group (NIAG)
Paul Scherrer Institut
CH-5232 Villigen PSI
Switzerland

Peter Niemz
ETH Zurich
Institute for Building Materials, Wood Physics
Schafmattstrasse 6
8093 Zurich
Switzerland